Eur. Phys. J. B **18**, 275–282 (2000)

THE EUROPEAN PHYSICAL JOURNAL B

EDP Sciences

Phase transitions in the mixed Ashkin-Teller model

S. Bekhechi, A. Benyoussef[a], A. El kenz, B. Ettaki, and M. Loulidi

Laboratoire de Magnétisme et de Physique des Hautes Énergies, Département de Physique, BP 1014, Faculté des Sciences, Rabat, Morocco

Received 5 July 1999 and Received in final form 4 July 2000

Abstract. By using a mean-field approximation (MFA) and Monte-Carlo (MC) simulations, we have studied the effect on the phase diagrams of mixed spins ($\sigma = 1/2$ and $S = 1$) in the Ashkin-Teller model (ATM) on a hypercubic lattice. By varying the strength describing the four spin interaction and the single ion potential, we have obtained by these two methods quite rich phase diagrams with several multicritical points. This model exhibits a new partially ordered phase $\langle S \rangle$ which does not exist neither in the spin-1/2 ATM nor in the spin-1 ATM. While MFA yields phase diagrams which are sometimes qualitatively incorrect, accurate results are obtained from MC simulations. From the critical exponents which have been calculated using finite-size scaling ideas, we have shown that all phase transitions are Ising-like except for the paramagnetic-Baxter critical surface on which the critical exponents vary continuously, by varying only the strength of the coupling interaction independently of the value of the single ion potential.

PACS. 75.10.Hk Classical spin models

1 Introduction

The Ashkin-Teller model [1] (A.T.M.) is a generalization of the Ising model to four component systems. It may be considered as a superposition of two Ising models, which are described by variables σ_i and S_i sitting on each of the sites on a hypercubic lattice. Within each Ising model, there is a two spin nearest-neighbour interaction with strength K_2. In addition, the different Ising models are coupled by a four spin interaction with strength K_4. Different methods have been applied to study the critical behaviour of this model [2–9]. All these methods yield three different phases: a paramagnetic (P) phase in which neither σ nor S nor anything's else is ordered ($\langle\sigma\rangle = \langle S\rangle = \langle\sigma S\rangle = 0$); a Baxter phase in which σ and S independently order in a ferromagnetic fashion and also $\langle\sigma S\rangle$ is unequal to zero; and a third phase called PO_1 in which σS is ordered ferromagetically, $\langle\sigma S\rangle \neq 0$, but $\langle\sigma\rangle = \langle S\rangle = 0$. Apart from the variational approaches which give a tricritical point, the other accurate methods yield only a line of critical points which connects the Ising critical point at one end to the four state Potts critical point at the other end, and along this line the exponents vary continuously [2,9]. A good physical realization for this model is the compound of Selenium adsorbed on a $\mathrm{N_i}$ surface. In this context, Per Bak *et al.* [2] have shown by using symmetry considerations that the order parameters σ and S transform as two-dimensional representations of the 4 pmm [10] symmetry group of the Ni(100) surface, and the phase transition belongs to the universality class of the xy model with cubic anisotropy as does the transition in the Ashkin-Teller model. The order parameter $\langle\sigma S\rangle$ transforms as a one-dimensional representation of the Ni(100) symmetry group and so the melting line is of Ising character.

One of the most interesting and challenging phenomena is the appearance of other new partially ordered phases in the ATM, such as: (i) the $\langle\sigma\rangle$ phase defined by $\langle\sigma\rangle \neq 0$ and $\langle S\rangle = \langle\sigma S\rangle = 0$ in the three-dimensional antiferromagnetic ATM [3]. (ii) The $\langle\sigma\rangle$ and $\langle S\rangle$ phases which are connected by a symmetry operation to the $\langle\sigma S\rangle$ phase in the bidimensional anisotropic ATM [11–13]. (iii) The PO_2 phase defined by ($\langle\sigma\rangle = \langle S\rangle \neq 0; \langle\sigma S\rangle = 0$) found recently in the spin-1 Ashkin Teller model [14,15].

The synthesis of single-chain and double-chain ferrimagnets is now becoming standard, and attempts to synthesize higher-dimensional polymeric ferrimagnets are starting to give very encouraging results. Some of the materials investigated are 2D organometallic ferrimagnets [16], 2D networks of the mixed-metal material $\{[\mathrm{P(Ph)_4}][\mathrm{MnCr(ox)_3}]\}_n$ where Ph is phenyl and ox is oxalate [17]. The intense activity related to the synthesis of ferrimagnetic materials requires a parallel effort in theoretical study. Mixed Ising spin systems provide a good model for studying ferrimagnetism [18,19].

In this paper we are mainly interested in the study of the isotropic mixed spins ($\sigma = 1/2,\ S = 1$) Ashkin-Teller model by using MFA and MC simulations. This model might be thought of either as describing ferrimagnets or adsorption phenomena. The paper is organized as follow. In the next section, the model is introduced and the ground state diagram is presented. Section 3 is devoted to the MFA description and the results are presented. Section 4 contains the formalism of the MC simulation and finite-size scaling theory. Our numerical results

[a] e-mail: benyous@fsr.ac.ma

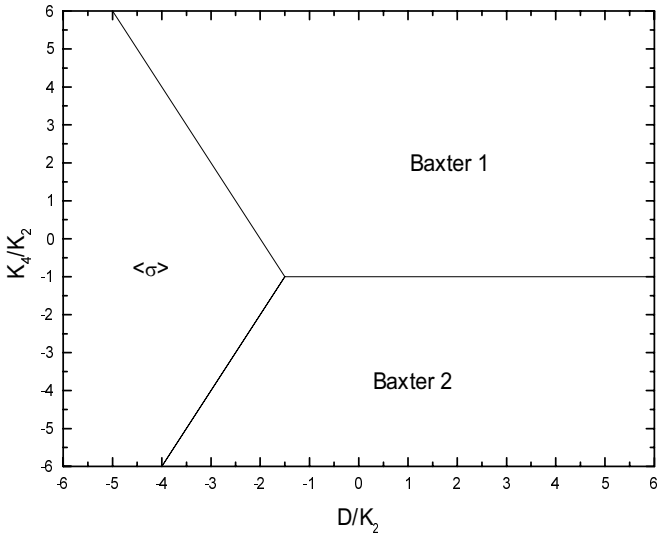

Fig. 1. Ground state phase diagram.

for the phase diagrams and the critical exponents are presented in Section 5. Finally, in Section 6 we conclude.

2 Model and ground state diagram

The model Hamiltonian used is given by:

$$H = -K_2 \sum_{\langle i,j \rangle} (\sigma_i \sigma_j + S_i S_j) - K_4 \sum_{\langle i,j \rangle} \sigma_i \sigma_j S_i S_j - D \sum_i S_i^2, \quad (1)$$

where the spins $S_i = \pm 1$, 0 and $\sigma_i = \pm 1/2$, are localized on the sites of a hypercubic lattice. The first term describes the bilinear interactions between the σ and S spins at sites i and j, with the interaction parameter K_2. The second term describes the four spin interaction with strength K_4, and on each site there is a single ion potential D. All these interactions are restricted to the z nearest-neighbours pairs of spins.

In order to calculate the ground state energy, we express the Hamiltonian as a sum of the contributions of the nearest-neighbours spins. So the contribution of a pair S_1, S_2 and σ_1, σ_2 is:

$$E_{\rm p} = -K_2(\sigma_1\sigma_2 + S_1 S_2) - K_4 \sigma_1 \sigma_2 S_1 S_2 - \frac{2D}{z}(S_1^2 + S_2^2). \quad (2)$$

By comparing the values of $E_{\rm p}$ for different configurations we obtain the following structure of phase diagram shown in Figure 1:

(i) For $D/K_2 \geq -3z/8$: if $K_4/K_2 > -1$ the Baxter1 phase is stable since both spins σ_i and S_i are aligned, otherwise if $K_4/K_2 < -1$ the spins σ_i are antiparallel while the spins S_i are parallel then we have: $\langle \sigma \rangle_{\rm F} = \langle S \rangle_{\rm AF} = \langle \sigma S \rangle_{\rm F} = 0$ and $\langle \sigma \rangle_{\rm AF} \neq 0$, $\langle S \rangle_{\rm F} \neq 0$ and $\langle \sigma S \rangle_{\rm AF} \neq 0$ which characterize the phase called Baxter2. The symbols $\langle \cdot \rangle_{\rm F}$ and $\langle \cdot \rangle_{\rm AF}$ indicate the thermal average of spin variables respectively in the ferromagnetic and antiferromagnetic phases.

(ii) For $D/K_2 < -3z/8$: We have two critical values of the single ion potential D, $Dc_1/K_2 = -z(1 - K_4/2K_2)/4$ and $Dc_2/K_2 = -z(1 + K_4/4K_2)/2$, such that if $D/K_2 < Dc_1/K_2$ and $D/K_2 > Dc_2/K_2$ the Baxter2 and Baxter1 phases are stable respectively. If $Dc_1/K_2 < D/K_2 < Dc_2/K_2$ the spins σ_i are parallel while the spins S_i are equal to zero then we have $\langle \sigma \rangle_{\rm F} \neq 0$, and $\langle S \rangle_{\rm F} = \langle \sigma S \rangle_{\rm F} = 0$ we obtain the phase called "$\langle \sigma \rangle$".

3 Mean-field approximation

The mean-field theory represents the infinite dimensional limit of statistical systems since it neglects correlations between different spins. However it is interesting to study the mean-field behaviour of the anisotropic A.T.M. so that we may effectively bracket the three-dimensional system between the mean- field and the $d = 2$ behaviour.

To write the mean-field equations let h_σ, h_S and $h_{\sigma S}$ denote the molecular fields associated with the order parameters $\langle \sigma \rangle$, $\langle S \rangle$ and $\langle \sigma S \rangle$ respectively, and $j(i)$ represents the set of all nearest neighbours to the site i:

$$h_\sigma = \sum_{j(i)} \langle \sigma_{j(i)} \rangle K_2; \quad h_S = \sum_{j(i)} \langle S_{j(i)} \rangle K_2; \quad \text{and} \quad h_{\sigma S} = \sum_{j(i)} \langle \sigma_{j(i)} S_{j(i)} \rangle K_4. \quad (3)$$

The effective Hamiltonian of the system is:

$$H_0 = -\left(h_\sigma \sum_i \sigma_i + h_S \sum_i S_i + h_{\sigma S} \sum_i \sigma_i S_i \right). \quad (4)$$

It generates the following partition function:

$$Z_0 = 2\exp(\beta h_S + \beta D) \cosh \frac{1}{2}(\beta h_\sigma + \beta h_{\sigma S}) + 2\exp(-\beta h_S + \beta D) \cosh \frac{1}{2}(\beta h_\sigma - \beta h_{\sigma S}) + 2\cosh \frac{1}{2}\beta h_\sigma \quad (5)$$

where $\beta = 1/K_{\rm B}T$ is the inverse temperature.

The variational principle for the free energy per site is described by:

$$F \leq \Phi = \frac{-1}{\beta} \ln(Z_0) + \langle H - H_0 \rangle \quad (6)$$

and the order parameters which are the spin averages are given by:

$$
\begin{aligned}
m_\sigma &= \langle\sigma\rangle \\
&= \frac{\left(\begin{array}{l}\exp\beta(h_S+D)\sinh\frac{\beta}{2}(h_S+h_{\sigma S})+\\ \exp\beta(-h_S+D)\sinh\frac{\beta}{2}(h_S-h_{\sigma S})+\sinh\frac{\beta}{2}h_\sigma\end{array}\right)}{2\Delta} \\
m_S &= \langle S\rangle \\
&= \frac{\left(\begin{array}{l}\exp\beta(h_S+D)\cosh\frac{\beta}{2}(h_S+h_{\sigma S})-\\ \exp\beta(-h_S+D)\cosh\frac{\beta}{2}(h_S-h_{\sigma S})\end{array}\right)}{\Delta} \qquad (7) \\
m_{\sigma S} &= \langle\sigma S\rangle \\
&= \frac{\left(\begin{array}{l}\exp\beta(h_S+D)\sinh\frac{\beta}{2}(h_S+h_{\sigma S})-\\ \exp\beta(-h_S+D)\sinh\frac{\beta}{2}(h_S-h_{\sigma S})\end{array}\right)}{2\Delta}, \\
\Delta &= \exp\beta(h_S+D)\cosh\frac{\beta}{2}(h_S+h_{\sigma S}) \\
&\quad + \exp\beta(-h_S+D)\cosh\frac{\beta}{2}(h_S-h_{\sigma S})+\cosh\frac{\beta}{2}h_\sigma.
\end{aligned}
$$

However the total free energy can be written as:

$$
\begin{aligned}
\Phi = &-\sum_i \ln Z_0 + K_2\left(\sum_{\langle i,j\rangle}\langle\sigma_i\rangle\langle\sigma_j\rangle+\sum_{\langle i,j\rangle}\langle S_i\rangle\langle S_j\rangle\right) \\
&+ K_4\sum_{\langle i,j\rangle}\langle\sigma_i S_i\rangle\langle\sigma_j S_j\rangle. \qquad (8)
\end{aligned}
$$

Usually the solutions of equation (7) combined with equation (3) are not unique. We choose the ones that minimize the free energy (Eq. (8)) and then represent the pure phases. If the order parameters are continuous, the transition is of the second- order, while if they are discontinuous, the transition is of first-order.

Our MF results are presented in the plane $(K_4/K_2, T/K_2)$ for $D/K_2 = -2.0$, Figure 2. In order to describe the different entities in the phase diagrams, we will use the Griffiths notations for the multicritical points [12,20]. At high temperature, the ordered phases (Baxter1 and Baxter2) are separated from the paramagnetic phase by the partially ordered phases $\langle\sigma S\rangle_{\rm F}$ and $\langle\sigma S\rangle_{\rm AF}$ at high absolute values of K_4/K_2. It appears also that lines of first order which are linked by triple points A^3, join the second order ones by tricritical point C and multicritical point BA^2 at high and low absolute values of K_4/K_2. At low temperature, the ordered phase $\langle\sigma\rangle$ which exists at the ground state is separated from the two other ordered (Baxter1 and Baxter2) and paramagnetic phases by first and second order phase transitions respectively. Since the MFA provides a qualitative picture of the phase diagram, we will present detailed studies using MC simulations.

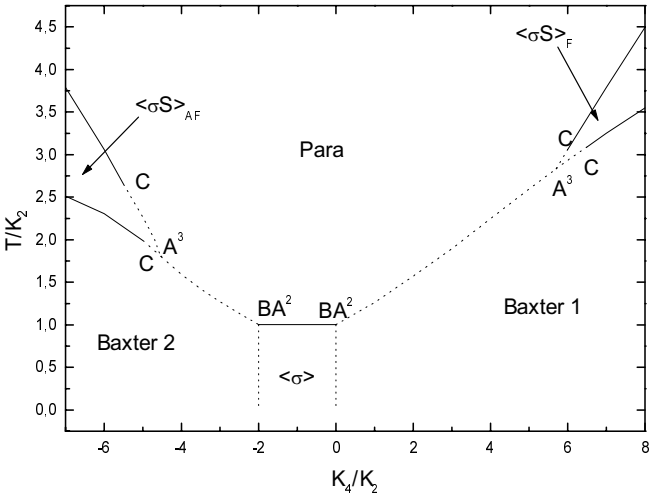

Fig. 2. Phase diagram for $D/K_2 = -2$ as obtained from mean field approximation. Solid and dashed lines denote second and first order phase transitions respectively. C, A^3 and BA^2 denote respectively tricritical points, triple points and critical end points.

4 Monte-Carlo simulations

The system studied is a $L \times L$ square lattice with even values of L, containing $N = L^2$ spins, and we use the well-known Metropolis algorithm [21] with periodic boundary conditions to update the lattice configurations. Monte-Carlo (MC) simulations are performed for $d = 2$ with systems of sizes $L = 8, 16, 24, 32$ and 64. We use 95 000 to 700 000 MC steps to calculate the thermodynamic quantities after discarding 5 000–50 000 sweeps for thermal equilibrium. Most of the phase diagrams presented here are obtained with $L = 32$ and are compared with those derived from MFA.

We can evaluate the stationary phase diagram of the model and its associated critical exponents by using the finite-size scaling concepts [22] applied to some thermodynamic properties of the system. The physical quantities of use are the magnetizations $|M_\alpha|(\alpha = \sigma, S, \sigma S)$, and are estimated by:

$$
|M_\alpha| = \langle|M_\alpha|\rangle = \frac{1}{Np}\sum_c\sum_i \alpha_i(c) \text{ with } \alpha = \sigma, S, \sigma S, \quad (9)
$$

where i runs over the lattice sites, c runs over the configurations obtained to update the lattice over one sweep of the N spins of the lattice (one Monte-Carlo step, MCS) counted after the system reaches thermal equilibrium, and p is the number of the MCS.

In order to measure the phase boundaries we will find useful the measurement of fluctuations (variance of the order-parameters) in M_α defined by the magnetic susceptibility:

$$
\chi_\alpha = \frac{N}{K_{\rm B}T}\left(\langle M_\alpha^2\rangle - \langle|M_\alpha|\rangle^2\right) \quad \text{with} \quad \alpha = \sigma, S, \sigma S. \qquad (10)
$$

The fourth-order cumulant $U_\alpha(\alpha = \sigma, S, \sigma S)$ are defined by:

$$U_\alpha = 1 - \frac{\langle M_\alpha^4 \rangle}{3\langle M_\alpha^2 \rangle^2} \cdot \tag{11}$$

Finally, we will use finite-size-scaling theory [21–23] to analyse our results. Following this approach, in the neighbourhood of the infinite critical point T_c, the above quantities obey for sufficiently large L:

$$|M_\alpha|_L(T) = L^{-\beta/\nu} M_0(L^{1/\nu}\varepsilon), \tag{12}$$

$$\chi_{\alpha L}(T) = L^{\gamma/\nu} \chi_0(L^{1/\nu}\varepsilon), \tag{13}$$

$$U_{\alpha L}(T) = U_0(L^{1/\nu}\varepsilon), \tag{14}$$

where $\varepsilon = T - T_c$.

If we derive equation (14) with respect to the temperature T, we obtain the scaling relation:

$$U'_\alpha(T) = L^{1/\nu} U'_0(L^{1/\nu}\varepsilon), \tag{15}$$

so that $U'_\alpha(T_c) = L^{1/\nu} U'_0(0)$. Then we can find the critical exponent ν from the log-log plot of $U'_L(Tc)$ *versus* L.

A first-order transition is signalled by hysteresis and discontinuous jumps in the internal energy ($E = \langle H \rangle$) and/or the order parameter (as will be shown in the next section). The first and second order transitions may be distinguished by the buildup of the magnetization by quenching the system from a disordered state (corresponding to an equilibrium configuration at very high temperature) to a temperature just below the transition temperature [21,23]. Due to the presence of long-lived metastable states, a two-step relaxation process is expected in the case of a first order transition, whereas a smooth buildup is observed in the case of continuous transition.

5 Results and discussion

5.1 Phase diagrams

A rich variety of phase transitions is observed by varying the strength of the coupling parameters.

- For $D/K_2 = -2.0$, our MC results are presented in the plane (K_4/K_2, T/K_2), Figure 3. At high temperature, the ordered phases (Baxter1 and Baxter2) are separated from the paramagnetic phase by the partially ordered phases $\langle \sigma S \rangle_F$ and $\langle \sigma S \rangle_{AF}$ at high absolute values of K_4/K_2. At intermediate values of K_4/K_2, the MC results present a new partially ordered phase called $\langle S \rangle$ whereas in the MF ones this latter phase is absent (see Fig. 2). This new phase, defined by $\langle \sigma \rangle = \langle \sigma S \rangle = 0$ and $\langle S \rangle \neq 0$, does not exist neither in the spin-1/2 [3] nor in the spin-1 [13] AT models. The variation of the order parameters and their susceptibilities are shown in Figure 4. The MC results are obtained from the maxima in the susceptibility and are qualitatively better than those of the MF ones and all the MC transition lines are of second order linked by multicritical points B^3 and B^2A, along all these lines

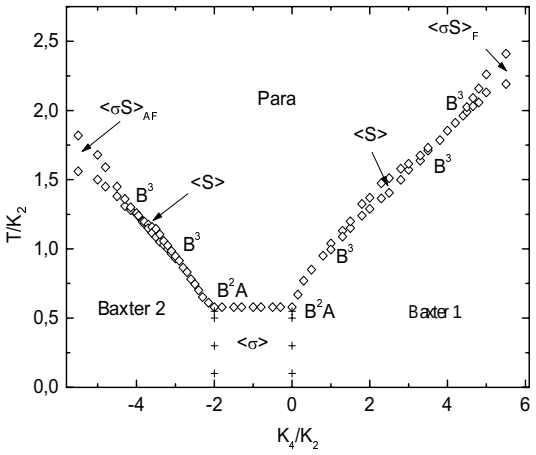

Fig. 3. Phase diagram for $D/K_2 = -2$ as obtained from MC simulations, where diamonds and plus denote second and first order phase transitions respectively. There is a multicritical point B^3 and a critical end point B^2A.

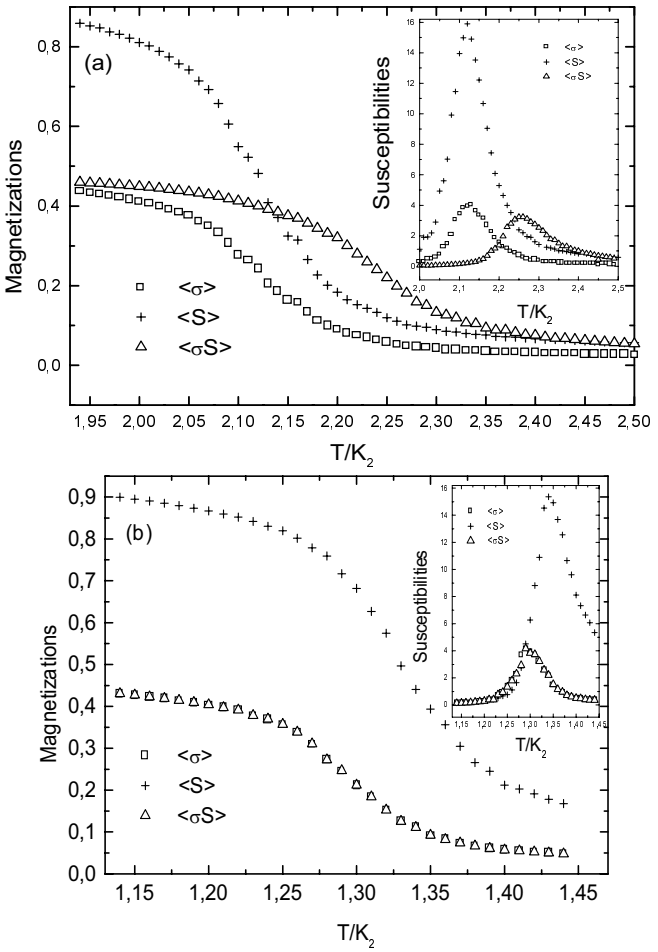

Fig. 4. Plot of order parameters $\langle \sigma \rangle$, $\langle S \rangle$ and $\langle \sigma S \rangle$ for $D/K_2 = -2.0$ from MC simulations, showing the existence of two new partially ordered phases at high temperature. The corresponding inset shows associated susceptibilities. a) $K_4/K_2 = 5$, existence of the $\langle \sigma S \rangle$ phase where at $T_1 = 2.13$, $\langle \sigma \rangle = \langle S \rangle = 0$ but $\langle \sigma S \rangle \neq 0$ whereas at $T_2 = 2.26$ we have $\langle \sigma \rangle = \langle S \rangle = \langle \sigma S \rangle = 0$. b) $K_4/K_2 = 2$, existence of the $\langle S \rangle$ phase where at $T'_1 = 1.29$, $\langle \sigma \rangle = \langle \sigma S \rangle = 0$ but $\langle S \rangle \neq 0$ whereas at $T'_2 = 1.34$ we have $\langle \sigma \rangle = \langle S \rangle = \langle \sigma S \rangle = 0$.

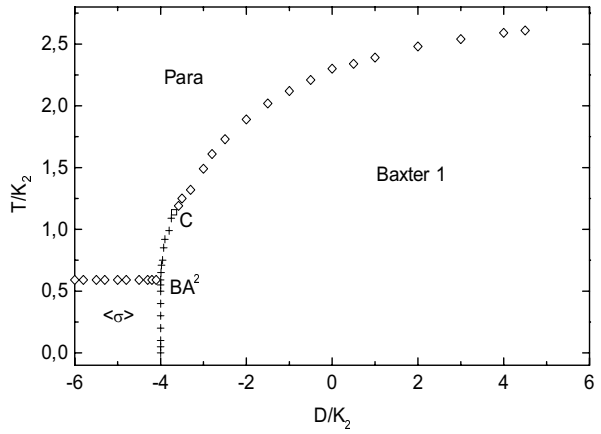

Fig. 5. Phase diagram for $K_4/K_2 = 4.0$ as obtained from MC simulations. Diamonds and pluses denote second and first order phase transitions respectively. In the phase diagram, there is a critical end point BA^2 and a tricritical point C denoted by a square and located at ($D/K_2 = -3.65 \pm 0.01$, $T/K_2 = 1.13 \pm 0.01$).

we didn't observe any hysteresis in the order parameters when crossing the boundaries (an example is shown below). Whereas in the MF phase diagram it appears also lines of first order which are linked by triple points A^3 and join the second order ones by tricritical point C and multicritical point BA^2 at high and low absolute values of K_4/K_2. At low temperature, the ordered phase $\langle\sigma\rangle$ which exists at the ground state is separated from the two other ordered (Baxter1 and Baxter2) and paramagnetic phases by first and second order critical lines respectively. As we can see in Figure 3, the $\langle S\rangle$ phase region is small for this value of D/K_2. Then in order to enlarge this region we have fixed the four spin interaction K_4/K_2 and varied the crystal field D/K_2. Also we note that only MC results are presented, since the MF ones are qualitatively similar with few differences in the multicritical points and the order of magnitude in the temperature transition which is higher as seen in the proceeding paragraph.

- For $K_4/K_2 = 0$ (we do not present the plots here) the mixed ATM is decoupled into the two well known independent spin-1/2 Ising model and spin-1 Blume-Capel model. The structure of the phase diagram is obtained by superposing the phase diagrams of these models. At high temperature and for all values of $D/K_2 > -2$, we obtain the $\langle S\rangle$ phase which is sandwiched between the Baxter1 and the paramagnetic phases. Its region of stability is enlarged for higher values of D/K_2. Whereas for $D/K_2 < -2$, we have only the $\langle\sigma\rangle$ and paramagnetic phases separated by a second order transition. At low temperature the two ordered phases $\langle\sigma\rangle$ and Baxter1 are separated by a first order transition.

- By increasing the strength of the four spin interaction $K_4/K_2 > 0$, the $\langle S\rangle$ region decreases and appears only at a high crystal field D/K_2, until a critical value of $K_4/K_2 = 4$, is reached. Then the $\langle S\rangle$ phase disappears and we have only a critical line with tricritical point which separates the Baxter1 phase ($\langle\sigma\rangle = \langle S\rangle = \langle\sigma S\rangle$) from the paramagnetic phase, Figure 5. Along the first-order line strong hysteresis was observed. The tricritical

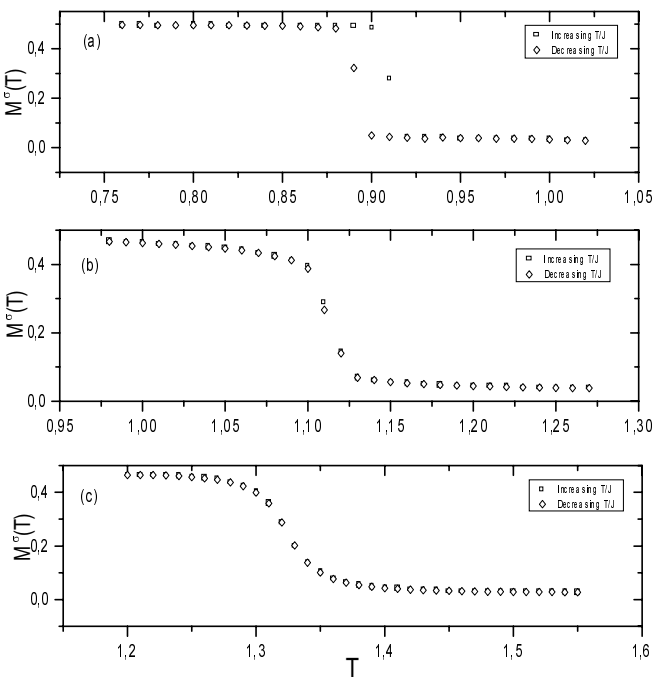

Fig. 6. Plot of order parameters $\langle\sigma\rangle$ *vs.* T/K_2 for $K_4/K_2 = 4$. (a) Typical hysteresis observed when crossing the first order transition boundary for $D/K_2 = -3.9$, we show also the discontinuity indicative of a first order transition. (b) By increasing the critical field, $D/K_2 = -3.68$, the hysteresis becomes very small and the behaviour of the order parameter is between first and second order transitions. At $D = -3.3$ the hysteresis behaviour disappears and we have also a continuity in the order parameter which is characteristic of a second order transition.

point was determined when the hysteresis disappears, Figures 6; it occurs, for $L = 32$, at ($D/K_2 = -3.65 \pm 0.01$, $T/K_2 = 1.13 \pm 0.01$). We note that the location of this tricritical point is not performed by a finite size scaling.

When the four coupling becomes very strong, $K_4/K_2 > 4$, Figure 7, the phase diagram exhibits the other partially ordered phase $\langle\sigma S\rangle_{\rm F}$ defined by $\langle\sigma\rangle = \langle S\rangle = 0$ and $\langle\sigma S\rangle \neq 0$, instead of the $\langle S\rangle$ phase. The former phase which appears at high crystal field is the same as the known partially ordered phase that occurs in the usual spin-1/2 ATM, since for large D the Hamiltonian (Eq. (1)) is reduced to the spin-1/2 ATM for which the $\langle\sigma S\rangle$ phase is favoured for strong values of the four spin interactions K_4. By decreasing the strength of the crystal field D/K_2, the transition between the Baxter 1 and the paramagnetic phases becomes of first order with a tricritical point C.

5.2 Critical behaviour

In the previous section we have described the general characteristics of different varieties of phase diagrams. Since it is important to determine the universality class of the critical boundaries we will focus ourselves to calculate the critical exponents.

In order to calculate the critical exponents of the Baxter1-disorder critical line and locate better the critical

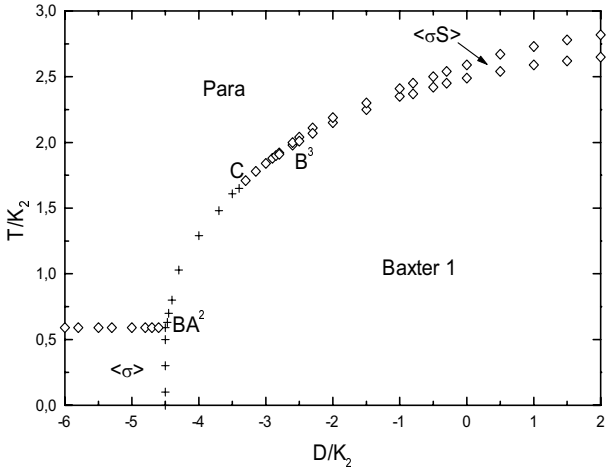

Fig. 7. Phase diagram for $K_4/K_2 = 5.0$ as obtained from MC simulations. Diamonds and pluses denote second and first order phase transitions respectively. B^3, C and BA^2 denote respectively multicritical point, tricritical point and critical end point.

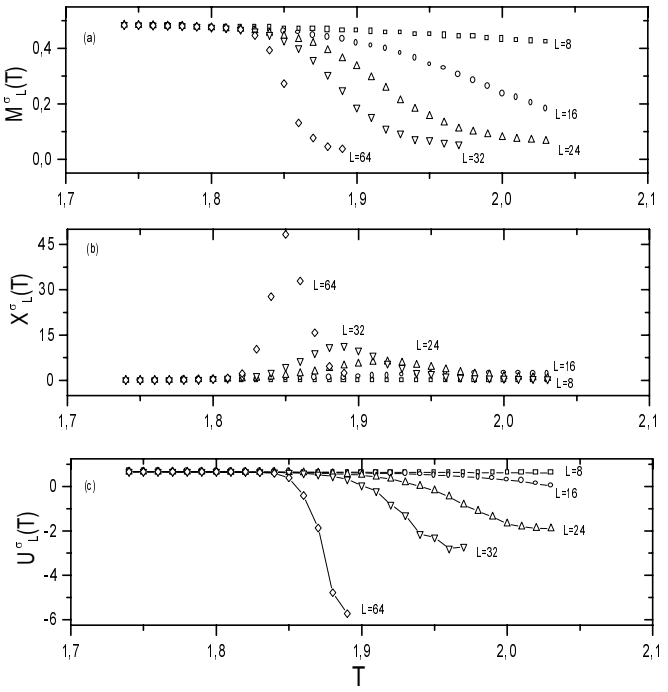

Fig. 8. Plots of the temperature variation T/K_2 for $K_4/K_2 = 4.0$ and $D/K_2 = -2$, for various choices of L, of: (a) the fourth-order cumulant. The critical temperature T_c is determined when all curves of $U_\alpha(T)$ intercept themselves. We estimate the value of T_c as being 1.83 ± 0.01. (b) Location of the susceptibility peak as the finite lattice critical temperature $T_c(L) = 1.85 \pm 0.01 : T_c(L) \to T_c$ when L increase. (c) The order parameters $\langle\sigma\rangle$ (Similar behaviours are obtained for $\langle S\rangle$ and $\langle\sigma S\rangle$).

temperature T_c of the model for $K_4/K_2 = 4$ and $D/K_2 = -2$ we plot in Figures 8 the magnetization, the susceptibility and the cumulant defined by equations (10–12) as a function of temperature T, for several values of L. The scaling relation for the fourth-order cumulant shows that, at the critical temperature, all curves of $U_\alpha(T)$ must intercept themselves at T_c for whatever value of L. From the latter figure we estimate the value of T_c as being 1.83 ± 0.01. With T_c determined we could now evaluate the critical exponents of the model. In Figure 9, we exhibit, at the critical temperature T_c, the log-log plot of the staggered magnetization, $M_\alpha(T_c)$, the susceptibility $\chi_\alpha(T)$ and the derivative of the cumulant $U'_\alpha(T_c)$ *versus* L. From the slope of the straight line, which is the best fit to the data points, and using equations (13, 14, 15), we can obtain the value of the stationary critical ratios β/ν, γ/ν and $1/\nu$ which are associated respectively to $M_\alpha(T_c)$, $\chi_\alpha(T)$ and $U'_\alpha(T_c)$. They are given in the table below. We can also estimate the ratio γ/ν by a log-log plot of the maximum value of the susceptibility *versus* L that is also scaled as $L^{\gamma/\nu}$ (Fig. 9b). The value we obtain is $\gamma/\nu = 1.745 \pm 0.002$. By the same way the critical temperature for $D/K_2 = 0.5$ was located at $T_c = 2.34 \pm 0.01$ and the critical exponents (see Tab. 1) are given from the finite size Scaling analysis.

At the tricritical point, with T_c determined ($T_c/K_2 = 1.13 \pm 0.01$) our best fits give $\nu_t = 0.556 \pm 0.013$, Figure 10a.

Another way to find the critical exponent ν is to use the location of the susceptibility peak as the finite lattice critical temperature $T_c(L)$, then $T_c(L) - T_c = L^{-1/\nu}$. The results obtained (Fig. 10b), $\nu_t = 0.55 \pm 0.013$, are consistent with the previous ones. All our results show that for $K_4/K_2 = 4$, the critical line belongs to the Ising critical and tricritical universality classes ($\beta/\nu = 1/8$, $\gamma/\nu = 7/4$, $\nu = 1$ [24,25], and $\nu_t = 5/9$ [26,27]).

For $K_4/K_2 = 0.25$, $D/K_2 = -2$, the model (Eq. (1)) becomes equivalent to the four state Potts model as confirmed in Figure 11 from the estimate of ν, $\nu = 0.664 \pm 0.01$, which is close to the four-state Potts critical exponents $\nu = 2/3$ [28]. By increasing K_4/K_2 the critical exponent ν varies until it reaches the value of the critical exponent Ising model $\nu = 1$ for $K_4/K_2 \to \infty$. We note that the critical exponent ν depends only on the value of K_4/K_2. It remains independent of D/K_2 which just extends the critical exponents from points (in the case of spin 1/2 ATM) to lines with tricritical exponents in addition as shown in reference [15] (spin-1 ATM). We conclude that the critical exponents vary continuously on the Baxter- paramagnetic critical surface in the same manner as in the spin 1/2 ATM (Ref. [9]) independently of the ratio D/K_2.

6 Conclusion

In this paper, we have shown by using MFA and MC simulations that the mixed ATM presents as well as the partially ordered phase $\langle\sigma S\rangle$ another new partially ordered phase $\langle S\rangle$ which does not exist neither in the spin-1/2 ATM nor in spin-1 A.T.M. The MC simulations give rich

Table 1. The critical exponents for $K_4/K_2 = 4$.

Critical exponents:	β/ν	γ/ν	ν
$D/K_2 = -2$	0.124 ± 0.003	1.765 ± 0.008	0.994 ± 0.007
$D/K_2 = 0.5$	0.126 ± 0.003	1.719 ± 0.04	0.992 ± 0.02
Exact results [24,25]	1/8	7/4	1

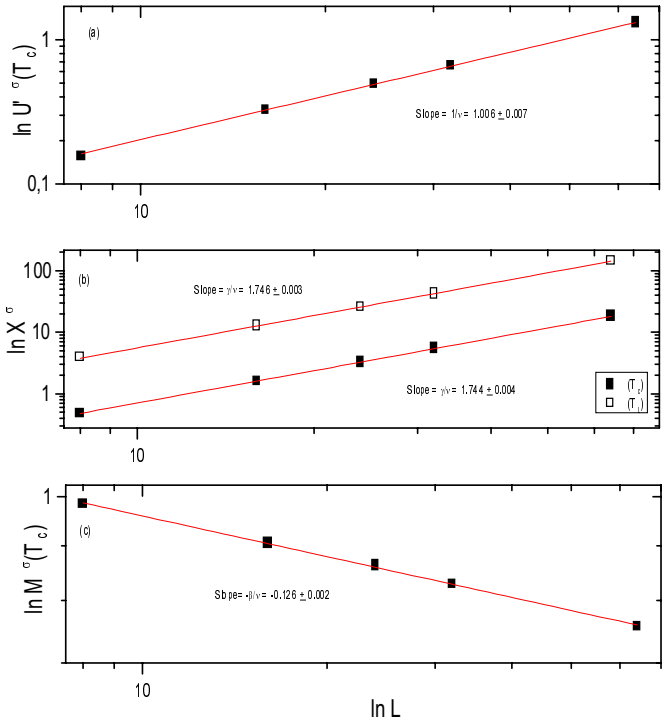

Fig. 9. Finite-size dependence of critical behaviour for $K_4/K_2 = 4.0$ and $D/K_2 = -2$ in log-log plots: (a) $U'(\sigma)(T_c)$ *vs.* L. The straight line is the best fit to the data points which gives: $\nu = 1.021 \pm 0.002$. (b) The susceptibility $\chi(\sigma)(T_c)$ at $T = T_c$ *vs.* L. The straight line is the best fit to the data points which gives: $\gamma/\nu = 1.765 \pm 0.008$. The susceptibility $\chi(\sigma)(T_L)$ at its maximum *vs.* L. The straight line is the best fit to the data points which gives: $\gamma/\nu = 1.745 \pm 0.002$. (c) The magnetization $M(\sigma)(T_c)$ *vs.* L. From the slope of the straight, which is the best fit to the data points, we obtain $\beta/\nu = 0.124 \pm 0.003$.

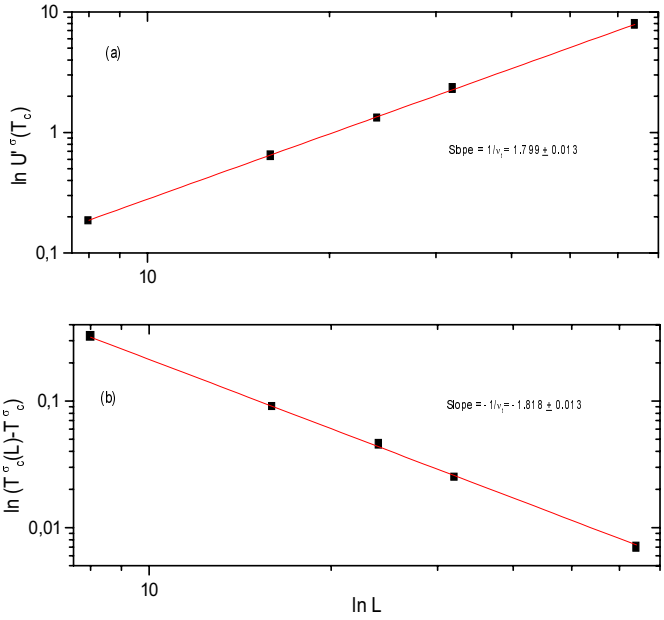

Fig. 10. At the critical point T_c for $K_4/K_2 = 4.0$ and $D/K_2 = -2$ a finite-size dependence in log-log plots: (a) $U'(T_c)$ *vs.* L. The straight line is the best fit to the data points which gives: $\nu_t = 0.556 \pm 0.013$. (b) $(T_c(L) - T_c)$ *vs.* L. The straight line is the best fit to the data points which gives: $\nu_t = 0.55 \pm 0.013$.

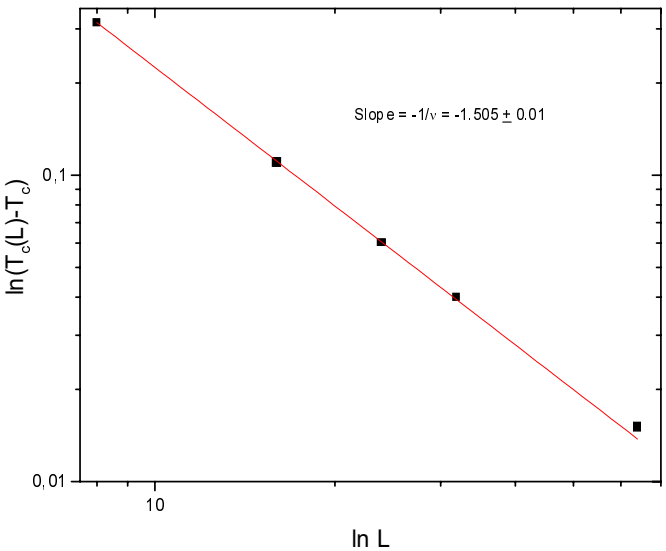

Fig. 11. $(T_c(L) - T_c)$ *vs.* L for $K_4/K_2 = 0.25$ and $D/K_2 = -2$. The straight line is the best fit to the data points which gives: $\nu = 0.664 \pm 0.01$.

phase diagrams with second and first order phase transitions which are more accurate and qualitatively better than those obtained by MFA. In the parameter space (K_4/K_2, D/K_2, T/K_2) the phase diagram presents rich varieties of phase transitions with surfaces of first and second order phase transitions which are bounded by lines of tricritical, triple and multicritical points. We have shown that all second order phase transitions are Ising-like while at the paramagnetic-Baxter phase transition the critical exponents vary continuously, by varying the strength of K_4/K_2 between the Ising and 4-state Potts critical exponents independently of the ratio D/K_2.

This work was supported by the PARS grant N°: Physique 035. One of the authors, (S.B.) thanks the Abdus Salam International Center For Theoretical Physics (ICTP) of Trieste for financial support.

References

1. J. Ashkin, E. Teller, Phys. Rev. **64**, 178 (1943).
2. P. Bak, P. Kleban, W.N. Unertel, J. Ochab, G. Akinci, N.C. Barlet, T.L. Einstein, Phys. Rev. Lett. **54**, 1539 (1985).
3. R.V. Ditzian, J.R. Banavar, G.S. Grest, L.P. Kadanoff, Phys. Rev. B **22**, 2542 (1980).
4. R.V. Ditzian, Phys. Lett. A **38**, 451 (1972).
5. F.J. Wegner, J. Phys. C **5**, L131 (1972).
6. J.R. Banavar, D. Jasnow, D.P. Landau, Phys. Rev. B **20**, 3820 (1979).
7. H.J.F. Knops, J. Phys. A **8**, 1508 (1975).
8. J.A. Plascak, F.C. Sà Barreto, J. Phys. A **19**, 2195 (1986).
9. S. Wiesman, E. Domany, Phys Rev. E **48**, 4080 (1993); S. Wiesman, E. Domany, Phys. Rev. E **51**, 3074 (1994).
10. D. Mukamel, E. Domany, M.E. Fisher, Phys. Rev. Lett. **37**, 565 (1976).
11. F.Y. Wu, K.Y. Lin, J. Phys. C **7**, L181 (1974).
12. .S. Bekhechi, A. Benyoussef, A. El kenz, B. Ettaki, M. Loulidi, Physica A **264**, 503 (1999).
13. M. Badehdah, S. Bekhechi, A. Benyoussef, M. Touzani, Physica B **291**, 394 (2000).
14. M. Loulidi, Phys. Rev. B **55**, 11611 (1997).
15. M. Badehdah, S. Bekhechi, A. Benyoussef, B. Ettaki, Phys. Rev. B **59**, 6052 (1999).
16. H. Tamaki, Z.J. Zhong, N. Matsumoto, S. Kida, M. Koikawa, N. Achiwa, Y. Hashimoto, H. Okawa, J. Am. Chem. Soc. **114**, 6974 (1992).
17. S. Decurtins, H.W. Schmalle, H.R. Oswald, A. Linden, J. Ensling, P. Gütlich, A. Hauser, Inorg. Chim. Acta. **65**, 216 (1994).
18. G. Ming, C. Zhang Yang, Phys. Rev. B **48**, 9452 (1993).
19. G.M. Buendia, M.A. Novothy, J. Phys. Cond. Matter. **9**, 5951 (1997).
20. R.B. Griffiths, Phys. Rev. B **12**, 345 (1975).
21. K. Binder, in *Applications of the Monte-Carlo Method in statistical physics*, edited by K. Binder (Springer-Verlag, Berlin, 1988).
22. V. Privman, *Finite-Size Scaling and Numerical Simulation of Statistical Systems* (World Scientific, Singapore, 1990).
23. D.P. Landau, K. Binder, Phys. Rev. B **17**, 2328 (1978); J.D. Kimel, S. Black, P. Carter, Y.L. Wang, Phys. Rev. B **35**, 3347 (1987); S. Bekhechi, A. Benyoussef, Phys. Rev. B **56**, 13954 (1997).
24. H.E. Stanley, *Introduction to phase Transitions and Critical Phenomena* (Oxford University Press, 1971).
25. B.M. McCoy, T.T. Wu., *The Two dimensional Ising Model* (Harvard University Press, Cambridge, MA, 1973).
26. M.P.M. den Nijs, J. Phys. A **12**, 1857, (1979).
27. B. Nienhuis, E.K. Riedel, M. Schick, J. Phys. A **13**, L 189, (1980).
28. B. Nienhuis, in *Phase Transition and Critical Phenomena*, edited by C. Domb, L. Lebowitz (Academic Press, New York, 1987).